INSTITUTE OF PHYSICS PUBLISHING JOURNAL OF OPTICS A: PURE AND APPLIED OPTICS
J. Opt. A: Pure Appl. Opt. **3** (2001) S184–S189 PII: S1464-4258(01)27691-0

Coupled optical microcavities in one-dimensional photonic bandgap structures

Mehmet Bayindir[1], **C Kural and E Ozbay**

Department of Physics, Bilkent University, Bilkent, 06533 Ankara, Turkey

E-mail: bayindir@fen.bilkent.edu.tr

Received 7 August 2001, in final form 14 September 2001
Published 26 October 2001
Online at stacks.iop.org/JOptA/3/S184

Abstract
We present a detailed theoretical and experimental study of the evanescent coupled optical microcavity modes in one-dimensional photonic bandgap structures. The coupled-cavity samples are fabricated by depositing alternating hydrogenated amorphous silicon nitride and silicon oxide layers. Splitting of the eigenmodes and formation of a defect band due to interaction between the neighbouring localized cavity modes are experimentally observed. Corresponding field patterns and the transmission spectra are obtained by using transfer matrix method (TMM) simulations. A theoretical model based on the classical wave analogue of the tight-binding (TB) picture is developed and applied to these structures. Experimental results are in good agreement with the predictions of the TB approximation and the TMM simulations.

Keywords: Photonic bandgap, microcavity, localization, tight-binding approximation

1. Introduction

In recent years, there has been much interest in the physics and applications of one-dimensional spatially periodic, quasiperiodic and random photonic bandgap (PBG) structures [1, 2]. Localization of light in disordered and quasiperiodic photonic systems has been widely studied [3, 4]. Superluminal tunnelling through one-dimensional PBG materials has also inspired great interest [5–7]. Properties of metallo-dielectric one-dimensional PBG structures have been investigated [8–11]. By using one-dimensional PBG structures, many interesting applications have been reported, such as second-harmonic generation [12], pulse compression [13], optical limiting and switching [14, 15], filters [16, 17], and photonic band edge lasers [18]. Moreover, the modification of spontaneous emission from atoms placed in one-dimensional PBG structures has been demonstrated [19–22].

By introducing a defect into the PBG structures, it is possible to obtain highly localized cavity modes inside the photonic stop band, which is analogous to the impurity states inside the semiconductor bandgap [23]. Since high-quality cavities have a crucial role in most of the photonic-crystal-based applications, it is very important to investigate the properties of cavities in these structures. In recent years, coupled microcavities (CMCs) have been investigated [24], and used in various applications [22, 25, 26]. These structures consist of two or more planar Fabry–Perot microcavities which are coupled to each other.

In the present work, we give a detailed experimental and theoretical analysis of the CMCs in one-dimensional photonic crystals. These structures are composed of amorphous silicon nitride and silicon oxide multilayers with coupled Fabry–Perot microcavities. This paper is organized as follows: in section 2, we first develop the classical wave analogue of the tight binding (TB) approximation in photonic crystals. Then we derive expressions for the eigenmode splitting, dispersion relation and group velocity corresponding to the coupled microcavity structures. The measured resonant frequencies of the coupled microcavity modes will be compared with the transfer matrix method (TMM) simulations and the TB results in section 3.

[1] To whom correspondence should be addressed.

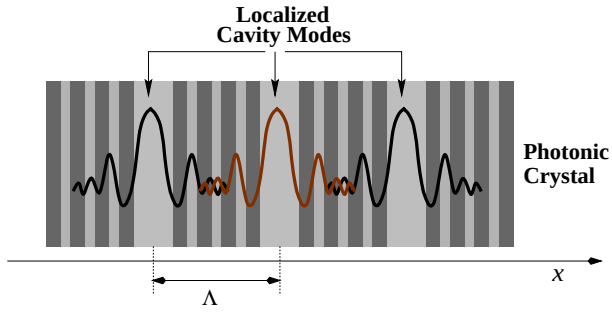

Figure 1. Schematic drawing of a coupled optical microcavity structure. A highly localized cavity mode interacts weakly with the neighbouring cavity modes, and therefore the electromagnetic waves propagate through coupled cavities.

2. Tight-binding description of localized modes in photonic crystals

Similarity between the Schrödinger equation and Maxwell's equations allows us to use many important tools which were originally developed for electronic systems. For example, it is well known that the TB method has proven to be very useful to study the electronic properties of solids [27]. Recently, the classical wave analogue of the TB picture [28] has successfully been applied to photonic structures [29–34]. By using direct implications of the TB picture, a novel propagation mechanism for photons along localized coupled cavity modes in photonic crystals was proposed [30, 33] and demonstrated [34, 35]. In these structures, photons can hop from one *tightly* confined mode to the neighbouring one due to the *weak* interaction between them (figure 1). We experimentally observed the mode splitting [34], waveguiding [35], heavy photons [36], and EM-beam splitting [37] in coupled-cavity systems in three-dimensional photonic crystals at microwave frequencies. In addition, we reported the strong enhancement of spontaneous emission throughout the cavity band of the one-dimensional coupled optical microcavity structures [22].

In this section, by using the TB approach [33, 34], we first obtain eigenvalues and eigenvectors corresponding to two and three CMCs (figure 1 shows the schematics of a one-dimensional coupled microcavity structure). Then, the expressions for dispersion relation and group velocity are derived. We first consider an individual localized mode $\boldsymbol{E}_\Omega(\boldsymbol{r})$ of a single cavity that satisfies a simplified version of the Maxwell equations

$$\nabla \times [\nabla \times \boldsymbol{E}_\Omega(\boldsymbol{r})] = \epsilon_0(\boldsymbol{r})(\Omega/c)^2 \boldsymbol{E}_\Omega(\boldsymbol{r}), \tag{1}$$

where $\epsilon_0(\boldsymbol{r})$ is the dielectric constant of the single cavity and Ω is the frequency corresponding to the cavity mode. Here it is assumed that $\boldsymbol{E}_\Omega(\boldsymbol{r})$ is real, nondegenerate and orthonormal; i.e., $\int \mathrm{d}\boldsymbol{r}\, \epsilon_0(\boldsymbol{r}) \boldsymbol{E}_\Omega(\boldsymbol{r}) \cdot \boldsymbol{E}_\Omega(\boldsymbol{r}) = 1$.

In the case of two weakly interacting coupled cavities, we can write the corresponding eigenmode as a superposition of the individual evanescent cavity modes as $\boldsymbol{E}_\omega(\boldsymbol{r}) = A\boldsymbol{E}_\Omega(\boldsymbol{r}) + B\boldsymbol{E}_\Omega(\boldsymbol{r} - \Lambda\hat{x})$. The eigenmode $\boldsymbol{E}_\omega(\boldsymbol{r})$ also satisfies equation (1) where $\epsilon_0(\boldsymbol{r})$ is replaced with the dielectric constant of the coupled system $\epsilon(\boldsymbol{r}) = \epsilon(\boldsymbol{r} - \Lambda\hat{x})$, and Ω replaced with eigenfrequency ω of the coupled cavity mode. Inserting $\boldsymbol{E}_\omega(\boldsymbol{r})$ into equation (1), and multiplying both sides from the left first by $\boldsymbol{E}_\Omega(\boldsymbol{r})$ and then by $\boldsymbol{E}_\Omega(\boldsymbol{r} - \Lambda\hat{x})$ and spatially integrating the resulting equations, we obtain the following eigenmodes and eigenfrequencies:

$$\boldsymbol{E}_{\omega_{1,2}}(\boldsymbol{r}) = \frac{\boldsymbol{E}_\Omega(\boldsymbol{r}) \pm \boldsymbol{E}_\Omega(\boldsymbol{r} - \Lambda\hat{x})}{\sqrt{2}}, \tag{2}$$

$$\omega_{1,2} = \Omega\sqrt{\frac{(1 \pm \beta)}{(1 \pm \alpha)}}, \tag{3}$$

where the TB parameters are given by $\alpha = \int \mathrm{d}\boldsymbol{r}\, \epsilon(\boldsymbol{r}) \boldsymbol{E}_\Omega(\boldsymbol{r}) \cdot \boldsymbol{E}_\Omega(\boldsymbol{r} - \Lambda\hat{x})$ and $\beta = \int \mathrm{d}\boldsymbol{r}\, \epsilon_0(\boldsymbol{r} - \Lambda\hat{x}) \boldsymbol{E}_\Omega(\boldsymbol{r}) \cdot \boldsymbol{E}_\Omega(\boldsymbol{r} - \Lambda\hat{x})$.

Similarly, the eigenmodes of three coupled cavities can be obtained as

$$\boldsymbol{E}_{\Gamma_2}(\boldsymbol{r}) = \frac{\boldsymbol{E}_\Omega(\boldsymbol{r}) - \boldsymbol{E}_\Omega(\boldsymbol{r} - 2\Lambda\hat{x})}{\sqrt{2}}, \tag{4}$$

$$\boldsymbol{E}_{\Gamma_{1,3}}(\boldsymbol{r}) = \frac{\boldsymbol{E}_\Omega(\boldsymbol{r}) \pm \sqrt{2}\,\boldsymbol{E}_\Omega(\boldsymbol{r} - \Lambda\hat{x}) + \boldsymbol{E}_\Omega(\boldsymbol{r} - 2\Lambda\hat{x})}{2}. \tag{5}$$

The corresponding eigenvalues are given by

$$\Gamma_2 = \Omega, \qquad \Gamma_{1,3} = \Omega\sqrt{\frac{1 \pm \sqrt{2}\beta}{1 \pm \sqrt{2}\alpha}}. \tag{6}$$

To derive equations (4)–(6), we ignore the second-nearest-neighbour coupling between the cavity modes. When we consider an array of cavities in which each cavity interacts weakly with neighbouring cavities, the eigenmode can be written as a superposition of the individual cavity modes

$$\boldsymbol{E}(\boldsymbol{r}) = E_0 \sum_n \mathrm{e}^{-\mathrm{i}nk\Lambda} \boldsymbol{E}_\Omega(\boldsymbol{r} - n\Lambda\hat{x}), \tag{7}$$

where the summation over n includes all the cavities. The dispersion relation for this structure can be obtained from equations (1) and (7) keeping only the nearest-neighbour coupling terms

$$\omega(k) = \Omega[1 + \kappa \cos(k\Lambda)]. \tag{8}$$

Here $\kappa = \beta - \alpha$ is a TB parameter which can be obtained from the splitting of the eigenmodes of two coupled cavities. After finding Ω, ω_1 and ω_2 from measurements or simulations, one can determine β and α by using equation (3).

The group velocity of photons along the localized coupled-cavity modes is given by

$$v_g(k) = \nabla_k \omega_k = -\kappa\Lambda\Omega \sin(k\Lambda). \tag{9}$$

Notice that all physical quantities including dispersion relation and group velocity depend on only a single TB parameter κ, and this parameter can be controlled by changing the properties of cavities and the intercavity distance.

3. Coupled optical microcavities: experiment versus theory

Five different samples are used to investigate the coupled optical microcavity structures. The first sample is a 15-pair

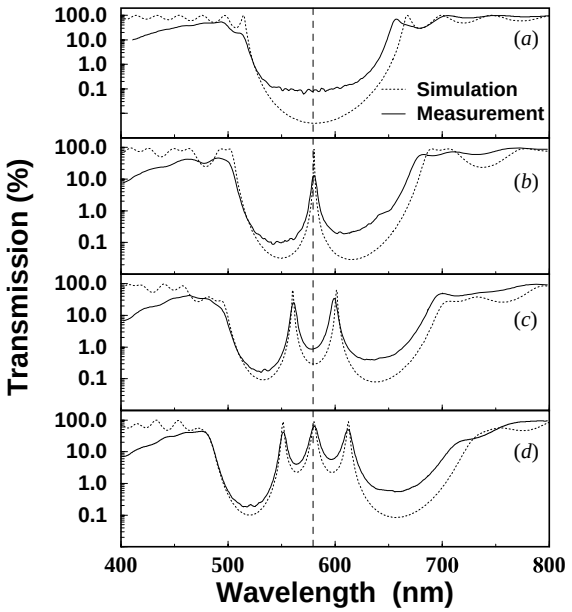

Figure 2. Measured (solid curves) and calculated (dotted curves) transmission spectra for (*a*) a DBR and (*b*) single-cavity, (*c*) two-coupled-cavity and (*d*) three-coupled-cavity structures. Due to coupling between the strongly localized microcavity modes, the single-cavity mode splits into two or three distinct modes depending on the number of coupled cavities. There is a good agreement between the measured and the calculated transmission spectra.

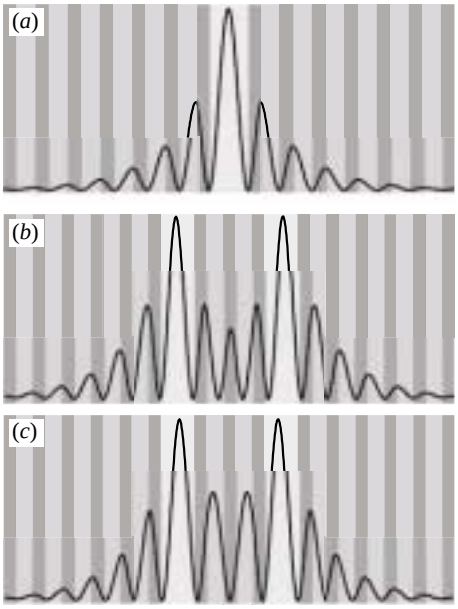

Figure 3. Calculated field patterns of a single cavity and two coupled cavities as a function of the position. (*a*) The field intensity corresponding to the single cavity for $\lambda = \lambda_0$ displays an oscillatory behaviour, and most of the field accumulates within the cavity region. (*b*), (*c*) The field intensities of two coupled cavities for resonant wavelengths (*b*) $\lambda = 560.6$ and (*c*) $\lambda = 601.6$. For both symmetric and antisymmetric cases, the field intensities exhibit peaks at the cavity regions.

distributed Bragg reflector (DBR). The other samples contain one, two, three and seven cavities, respectively. Each pair in these structures consists of $\lambda_0/4$ thick alternating silicon nitride (Si_3N_4) and silicon oxide (SiO_2) layers. The corresponding thicknesses and refractive indices are determined by using a Radolph AutoEL III ellipsometer as $d_{SiO_2} = 97.0$ nm, $d_{Si_3N_4} = 70.3$ nm and $n_{SiO_2} = 1.48$, $n_{Si_3N_4} = 2.10$. The cavity layers are silicon oxide with 194 nm ($\lambda_0/2$) thickness, and $\Lambda = 2.5$ pairs intercavity distance. These samples are grown on silicon and glass substrates by using the plasma-enhanced chemical vapour deposition (PECVD) technique at 250 °C. Nitrogen-(N_2-) balanced 2% silane (SiH_4), pure ammonia (NH_3) and nitrous oxide (N_2O) are used as the silicon, nitride and oxide sources, respectively. The transmission measurements are performed by using an Ocean Optics S2000 fibre spectrometer. The minimum value of the measured transmission, 0.1%, is due to the sensitivity of our experimental set-up. We also obtained the transmission characteristics and the field patterns of these fabricated structures by using the TMM [38].

The measured transmission spectrum of the DBR exhibits a forbidden gap extending from 515.3 to 654.2 nm. The simulation result agrees well with the measurement, and shows a stop band extending from 517.5 to 663.3 nm (figure 2(*a*)). In the presence of a single cavity, a highly localized cavity mode is observed within the PBG. The measured cavity wavelength appears at $\lambda_0 = 580.4$ nm ($\Omega_0 = c/\lambda_0 = 516.9$ THz), with a quality factor, defined as $\Delta\lambda/\lambda$, of $Q = 128$. As shown in figure 2(*b*), the TMM results in a resonant wavelength at 580.5 nm with $Q = 707$. The corresponding field pattern at the resonance wavelength $\lambda = \lambda_0$ for normal incidence is also calculated. Figure 3(*a*) shows the field intensity as function of position x (deposition direction). The localized cavity field, $|\boldsymbol{E}_\Omega(\boldsymbol{r})|^2$, exhibits an oscillatory behaviour, and most of the field is concentrated around the cavity region.

For two coupled cavities, the transmission characteristics as a function of wavelength are measured and calculated. As shown in figure 2(*c*), we observe that the resonance mode is split into two distinct symmetric and antisymmetric modes. The measured values of the resonance wavelengths are 599.3 nm ($\omega_1 = 500.6$ THz) and 561.1 nm ($\omega_2 = 534.7$ THz), which are very close to the calculated results, i.e. 601.6 and 560.6 nm. At this point, we can determine the TB parameters, α and β, by inserting measured or calculated values of ω_1 and ω_2 into equation (3). This procedure leads to a TB parameter $\kappa = -0.066$ when we use experimentally determined values of ω_1 and ω_2. Similarly, the corresponding resonant frequencies obtained by the TMM simulations lead to $\kappa = -0.07$, which is very close to the experimentally obtained value.

The calculated field patterns corresponding to these modes are plotted in figures 3(*b*) and (*c*). It is observed that although both field patterns show two peaks around the cavity regions they also exhibit different properties between the cavities. The field intensity corresponding to the lower-frequency mode (antisymmetric) has a node between the cavities. This result is along our expectations, as the localized photon modes should overlap when two isolated cavities are brought together. Due to this interaction, the doubly degenerate eigenmode splits into two distinct modes as we described in the previous section (see equation (2)) [39]. These modes are reminiscent of the bonding and antibonding states in solid state physics. For example, in the diatomic molecules, the interaction between the two atoms produces a splitting of the degenerate atomic levels into bonding and antibonding orbitals [40]. Recently, the splitting

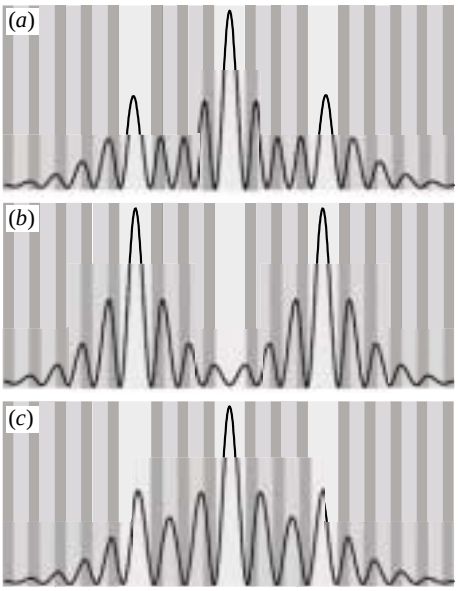

Figure 4. Calculated field patterns of three coupled cavities for the resonant wavelengths (*a*) $\lambda = \lambda_1$, (*b*) $\lambda = \lambda_2$ and (*c*) $\lambda = \lambda_3$. These modes can be constructed by the superposition of the individual cavity mode which is localized at each cavity site.

of photon modes has also been observed in photonic molecules which were fabricated by coupling pairs of micrometre-sized semiconductor cavities [41].

When we brought three cavities together, the single-cavity mode Ω_0 split into three different eigenmodes. In this case, the corresponding transmission spectra are measured and calculated. As shown in figure 2(*d*), there is good agreement between measured and calculated transmission characteristics of the three coupled cavities. Figure 4 exhibits corresponding field patterns of three coupled cavities. The first and third modes, figures 4(*a*) and (*c*), are linear combinations of three individual localized cavity modes with appropriate coefficients, which are given in equation (5). The second mode, figure 4(*b*), is obtained by combining only the first and third cavity modes, which corresponds to equation (4). As shown in figure 4, there is a exact correspondence between the calculated field patterns by using the TMM and predictions of the TB analysis.

We also compare the measured and the calculated resonant wavelengths of three CMCs with the TB approximation results, which are determined by inserting the parameters α and β (these parameters can be obtained from either measured or calculated values of ω_1 and ω_2 by using equation (3)) into the equation (6). Table 1 gives a comparison between the measured and calculated resonance wavelengths of three coupled cavities with the TB predictions. These parameters can be determined from the experiments and TMM simulations. The measured and calculated (by using the TMM code) values of the resonance frequencies coincide well with the TB approximation's predictions. This excellent agreement shows that the classical wave analogue of TB formalism is a useful tool to investigate PBG structures.

When more cavities are brought together, due to coupling between localized cavity modes, we expect that a cavity band is formed within the PBG. Figure 5(*a*) displays the measured

Table 1. Comparison of the resonant wavelengths of three coupled cavities obtained by measurements, the TMM simulations and the TB approximation. The measured results are in excellent agreement with the TMM simulation results, and the prediction of the TB approximation.

	Measurement	TMM	TB[a]	TB[b]
λ_1 (nm)	551.8	551.4	552.7	553.1
λ_2 (nm)	580.7	580.4	580.5	580.4
λ_3 (nm)	612.1	612.4	610.6	607.0

[a] Simulated results are used to determine α and β by using equation (3).
[b] Experimental results are used to determine α and β by using equation (3).

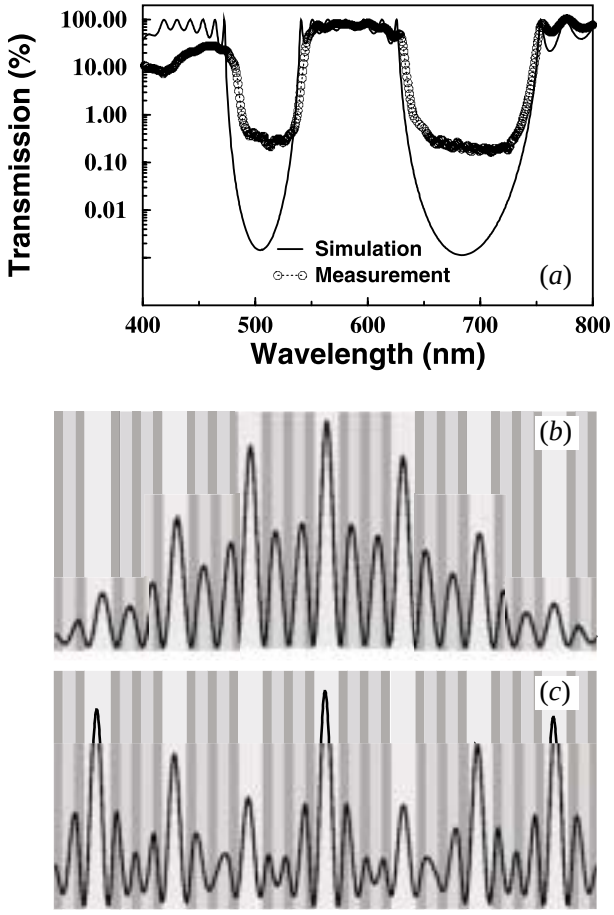

Figure 5. (*a*) Measured (circles) and calculated (solid curve) transmission through a coupled microcavity (CMC) structure which contains seven coupled cavities. A cavity band is formed between 530 and 659 nm. Nearly 100% transmission is observed throughout the cavity band. (*b*), (*c*) Calculated field patterns corresponding to two different wavelengths within the cavity band, namely (*b*) $\lambda = 628.3$ nm and (*c*) $\lambda = 567.0$ nm. The extended nature of these modes can be achieved by linear combination of localized cavity modes, where each of them is confined around the cavity region.

and simulated transmission spectra of CMC structures which contain seven cavities. The cavity band extends from 540 to 626 nm. Nearly 100% transmission is achieved throughout the cavity band. The calculated transmission spectra agree well with our measurements. It is important to note that since the cavity band edges are very sharp compared to

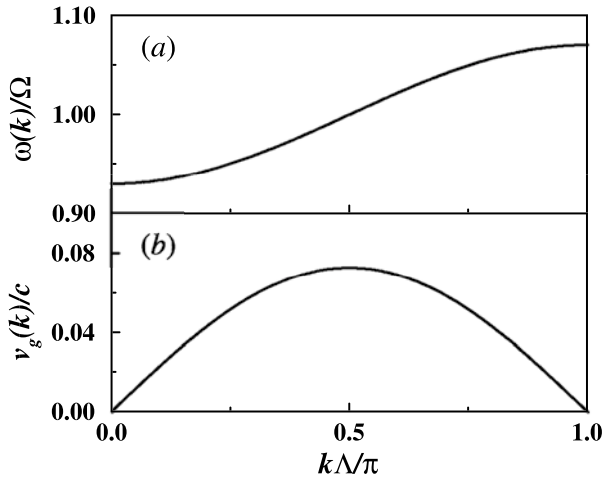

Figure 6. (*a*) Calculated dispersion relation of the CMC structure by using equation (8) with $\kappa = -0.07$. (*b*) The group velocity is plotted according to equation (9) as a function of wavevector k. The group velocity is one order of magnitude smaller than the speed of light at the band centre ($k\Lambda = \pi/2$), and vanishes at the band edges ($k\Lambda = 0$ and π).

the PBG edges, one can use this sharpness to construct photonic switches [15, 35]. Recently, Bayer *et al* [42] reported formation of a photonic band due to coupling between photonic molecules. The corresponding field intensity profiles for two different wavelengths within the cavity band are calculated. As shown in figures 5(*b*) and (*c*), the field intensity profiles look like extended modes which have nonzero values along the cavity sites.

We can obtain the dispersion relation of the CMC structure after finding the TB parameters from measurements or simulations. Figure 6(*a*) shows the calculated dispersion relation $\omega(k)$ as a function of wavevector k by using equation (8) with $\kappa = -0.07$. We also plotted the normalized group velocity (equation (9)) corresponding to the CMC. As shown in figure 6(*b*), the group velocity has its maximum value, nearly one-tenth of the speed of light, at the coupled-cavity band centre, and vanishes at the band edges. The coupled-microcavity structures can efficiently be used in certain applications such as dispersion compensators and photonic switches. Moreover, the spontaneous emission rate and the efficiency of nonlinear processes can be enhanced in coupled-microcavity systems due to very low group velocity.

4. Conclusions

In summary, the transmission properties of the coupled-microcavity structures in one-dimensional PBG materials have been investigated. The structures are fabricated by using hydrogenated amorphous silicon nitride and silicon oxide multilayers. The splitting of eigenmodes due to interaction between the localized electromagnetic cavity modes is observed. The TB parameters are extracted from measurements and the TMM simulation results.

Acknowledgments

This work was supported by NATO grant no SfP971970, National Science Foundation grant no INT-9820646, Turkish Department of Defence grant no KOBRA-001 and Thales JP8.04.

References

[1] Joannopoulos J D, Meade R D and Winn J N 1995 *Photonic Crystals: Molding the Flow of Light* (Princeton, NJ: Princeton University Press)
[2] For a recent review, see articles in Soukoulis C M (ed) 2001 *Photonic Crystals and Light Localization in the 21st Century* (Dordrecht: Kluwer)
[3] Gellermann W, Kohmoto M, Sutherland B and Taylor P C 1994 Localization of light waves in Fibonacci dielectric multilayers *Phys. Rev. Lett.* **72** 633–6
[4] Hattori T, Tsurumachi N, Kawato S and Nakatsuka H 1994 Photonic dispersion relation in a one-dimensional quasicrystal *Phys. Rev.* B **50** R4220–3
[5] Nimtz G 1997 *Tunneling and its Implications* ed A Ranfagin (Singapore: World Scientific)
[6] Spielmann Ch, Szipocs R, Stingl A and Krausz F 1994 Tunneling of optical pulses through photonic band gaps *Phys. Rev. Lett.* **72** 2308–11
[7] Pereyra P 2000 Closed formulas for tunneling time in superlattices *Phys. Rev. Lett.* **84** 1772–5
[8] Scalora M, Bloemer M J, Pethel A S, Dowling J P, Bowden C M and Manka A S 1998 Transparent, metallo-dielectric, one-dimensional, photonic band gap structures *J. Appl. Phys.* **83** 2377–83
[9] Bloemer M J and Scalora M 1998 Transmissive properties of Ag/MgF_2 photonic band gaps *Appl. Phys. Lett.* **72** 1676–8
[10] Sibilia C, Scalora M, Centini M, Bertolotti M, Bloemer M J and Bowden C M 1999 Electromagnetic properties of periodic and quasiperiodic one-dimensional, metallo-dielectric photonic band gap structures *J. Opt. A: Pure Appl. Opt.* **1** 490–4
[11] Bennink R S, Yoon Y-K and Boyd R W 1999 Accessing the optical nonlinearity of metals with metal^dielectric photonic bandgap structures *Opt. Lett.* **24** 1416–8
[12] Dolgova T V, Madikovski A I, Martemyanov M G, Marovsky G, Mattei G, Schuhmacher D, Yakovlev V A, Fedyanin A A and Aktsipetrov O A 2001 Giant second harmonic generation in microcavities based on porous silicon photonic crystals *JETP Lett.* **73** 6–9
[13] Andreev A V, Balakin A V, Ozheredov I A, Shkurinov A P, Masselin P, Mouret G and Boucher D 2000 Compression of femtosecond laser pulses in thin one-dimensional photonic crystals *Phys. Rev.* E **53** 016602
[14] Scalora M, Dowling J P, Bowden C M and Bloemer M J 1994 Optical limiting and switching of ultrashort pulses in nonlinear photonic band gap materials *Phys. Rev. Lett.* **73** 1368–71
[15] Lan S, Nishikawa S and Wada O 2001 Leveraging deep photonic band gaps in photonic crystal impurity bands *Appl. Phys. Lett.* **78** 2101–3
[16] Lei X-Y, Li H, Ding F, Zhang W and Ming N-B 1997 Novel application of a perturbed photonic crystal: high-quality filter *Appl. Phys. Lett.* **71** 2889–91
[17] Qiao F, Zhang C, Wan J and Zi J 2000 Photonic quantum-well structures: multiple channeled filtering phenomena *Appl. Phys. Lett.* **77** 3698–700
[18] Dowling J P, Scalora M, Bloemer M J and Bowden C M 1994 The photonic band edge laser: a new approach to gain enhancement *J. Appl. Phys.* **75** 1896–9
[19] Tocci M D, Scalora M, Bloemer M J, Dowling J P and Bowden C M 1996 Measurement of spontaneous emission

enhancement near the one-dimensional photonic band edge of semiconductor heterostructures *Phys. Rev.* A **53** 2799–03

[20] Giorgis F 2000 Optical microcavities based on amorphous silicon-nitride Fabry–Perot structures *Appl. Phys. Lett.* **77** 522–4

[21] Serpenguzel A and Tanriseven S 2000 Controlled photoluminescence in amorphous-silicon-nitride microcavities *Appl. Phys. Lett.* **78** 1388–90

[22] Bayindir M, Tanriseven S, Aydinli A and Ozbay E 2001 Strong enhancement of spontaneous emission in amorphous-silicon-nitride photonic crystal based coupled-microcavity structures *Appl. Phys. A: Mater. Sci. Process* **73** 125

Bayindir M, Tanriseven S and Ozbay E 2001 Propagation of light through localized coupled-cavity modes in one-dimensional photonic band gap structures *Appl. Phys. A: Mater. Sci. Process* **72** 117–9

[23] Yablonovitch E, Gmitter T J, Meade R D, Rappe A M, Brommer K D and Joannopoulos J D 1991 Donor and acceptor modes in photonic band structure *Phys. Rev. Lett.* **67** 3380–3

[24] Pavesi L, Panzarini G and Andreani L C 1998 All-porous silicon-coupled microcavities: experiment versus theory *Phys. Rev.* B **58** 15794–800

[25] Stanley R P, Houdre R, Oesterle U, Ilegems M and Weisbuch C 1994 Coupled semiconductor microcavities *Appl. Phys. Lett.* **65** 2093–5

[26] Hu S Y, Hegblom E R and Coldren L A 1997 Coupled-cavity resonant photodetectors for high-performance wavelength demultiplexing applications *Appl. Phys. Lett.* **71** 178–80

[27] Harrison W A 1980 *Electronic Structure and the Properties of Solids* (San Francisco: Freeman)

[28] Ashcroft N W and Mermin N D 1976 *Solid State Physics* (Philadelphia, PA: Saunders)

[29] de Sterke C M 1998 Superstructure gratings in the tight-binding approximation *Phys. Rev.* E **57** 3502–9

[30] Stefanou N and Modinos A 1998 Impurity bands in photonic insulators *Phys. Rev.* B **57** 12127–33

[31] Lidorikis E, Sigalas M M, Economou E N and Soukoulis C M 1998 Tight-binding parametrization for photonic band gap materials *Phys. Rev. Lett.* **81** 1405–8

[32] Mukaiyama T, Takeda K, Miyazaki H, Jimba Y and Kuwata-Gonokami M 1999 Tight-binding photonic molecule modes of resonant bispheres *Phys. Rev. Lett.* **82** 4623–6

[33] Yariv A, Xu Y, Lee R K and Scherer A 1999 Coupled-resonator optical waveguide: a proposal and analysis *Opt. Lett.* **24** 711–3

Xu Y, Lee R K and Yariv A 2000 Propagation and second-harmonic generation of electromagnetic waves in a coupled-resonator optical waveguide *J. Opt. Soc. Am.* B **17** 387–400

[34] Bayindir M, Temelkuran B and Ozbay E 2000 Tight-binding description of the coupled defect modes in three-dimensional photonic crystals *Phys. Rev. Lett.* **84** 2140–3

[35] Bayindir M, Temelkuran B and Ozbay E 2000 Propagation of photons by hopping: A waveguiding mechanism through localized coupled-cavities in three-dimensional photonic crystals *Phys. Rev.* B **61** R11855–8

[36] Bayindir M and Ozbay E 2000 Heavy photons at coupled-cavity waveguide band edges in a three-dimensional photonic crystal *Phys. Rev.* B **62** R2247–50

[37] Bayindir M, Temelkuran B and Ozbay E 2000 Photonic crystal based beam splitters *Appl. Phys. Lett.* **77** 3902–4

[38] Ghatak A and Thyagarajan K 1989 *Optical Electronics* (New York: Cambridge University Press)

[39] Antonoyiannakis M I and Pendry J B 1997 Mie resonances and bonding in photonic crystals *Europhys. Lett.* **40** 613–8

Antonoyiannakis M I and Pendry J B 1999 Electromagnetic forces in photonic crystals *Phys. Rev.* B **60** 2363–74

[40] Kittel C 1996 *Introduction to Solid State Physics* 7th edn (New York: Wiley) p 75

[41] Bayer M, Gutbrod T, Reithmaier J P, Forchel A, Reinecke T L, Knipp P A, Dremin A A and Kulakovskii V D 1998 Optical modes in photonic molecules *Phys. Rev. Lett.* **81** 2582–5

[42] Bayer M, Gutbrod T, Forchel A, Reinecke T L, Knipp P A, Werner R and Reithmaier J P 1999 Optical demonstration of a crystal band structure formation *Phys. Rev. Lett.* **83** 5374–7